

# Experimental Studies of CO<sub>2</sub> Sequestration in Ferric Iron-Bearing Sediments: CO<sub>2</sub>-SO<sub>2</sub> Reaction with Hematite

JAMES L. PALANDRI, ROBERT J. ROSENBAUER, AND YOUSIF K. KHARAKA  
U.S. Geological Survey, 345 Middlefield Rd., Menlo Park, CA 94025, USA

**Abstract**—Computer simulations of reactions among SO<sub>2</sub>-bearing, CO<sub>2</sub>-dominated gas and aqueous-mineral phases show that ferric iron in sediments can be converted almost entirely to dissolved ferrous iron and the iron carbonate mineral siderite, and that SO<sub>2</sub> can simultaneously be oxidized to dissolved sulfate. In parallel with the modeling, we carried out an experiment in a well stirred reactor with hematite, 1.0 m NaCl, SO<sub>2</sub> in quantity sufficient to reduce much of the iron, and excess CO<sub>2</sub>. Experimental results yield siderite, solid iron sulfide, native sulfur, un-reacted hematite, and due to aluminum-bearing impurities in the hematite, dawsonite. At 150°C and 300 bar, total dissolved iron, mostly ferrous, increases to 447 ppm after 25 days, decreases to 190 ppm after 40 days, then remains near constant until termination of the experiment at 57 days. The experiment did not reach equilibrium, as indicated by coexistence of metastable solid iron sulfide and metastable native sulfur with siderite. However, results confirm that ferric iron can be used to trap CO<sub>2</sub> in siderite, if reduced sulfur (as SO<sub>2</sub>) is present to reduce the iron with CO<sub>2</sub> in the gas phase.

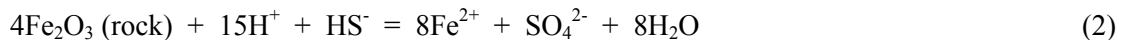
## 1. INTRODUCTION

Studies of in situ mineral trapping of CO<sub>2</sub> (Gunter et al., 1997, 2000; Johnson et al., 2001; Pruess et al., 2001) generally consider the use of Ca-bearing arkosic, Mg-bearing illitic, or Fe-bearing glauconitic sediments, to trap CO<sub>2</sub> in calcite, magnesite, siderite, or ankerite. Glauconitic beds, which contain the desired ferrous iron, are generally of limited thickness and geographical occurrence. However, ferric iron-bearing sediments, including redbeds, are of widespread geographic distribution, generally great thickness, with high porosity and permeability. As such, they have great potential to trap CO<sub>2</sub> in siderite and/or ankerite. However, iron must be in its ferrous oxidation state to precipitate in carbonate minerals.

Experimental and theoretical investigations of H<sub>2</sub>S sequestration in redbeds (Palandri, 2000) to dispose of H<sub>2</sub>S in sour natural gas, show that dissolved sulfide will react with ferric iron to produce amorphous iron sulfide and dissolved sulfate (eqn. (1))



and that the reaction attains 90% completion over time scales of days to weeks, depending primarily on the experimental temperatures of 28° to 71°C (Palandri, 2000). A significant result of this reaction is the steady increase in the concentration of dissolved ferrous iron to over 10000 ppm (eqn. (2))



despite its removal by iron sulfide precipitation as in eqn. (1)(Palandri, 2000). This ferrous iron is therefore available for precipitation in carbonate minerals.

Field observations of volcanic systems and thermodynamic modeling (Getahun et al., 1996; Symonds et al., 2001) show that SO<sub>2</sub> gas forms H<sub>2</sub>S and H<sub>2</sub>SO<sub>4</sub> in a disproportionation reaction (eqn. (3))



Given that flue gas from fossil fuel-fired power plants, especially those using coal, may contain up to 5 wt% of SO<sub>2</sub>, we investigate with geochemical modeling and laboratory experiments whether SO<sub>2</sub> can be used to reduce ferric iron to ferrous, and if fugacities of H<sub>2</sub>S and CO<sub>2</sub> can be maintained so that precipitation of iron carbonate is favored over iron sulfides (eqn. (4))



Previous geochemical equilibrium simulations show that the products in reaction (4) are favored under a wide range of conditions (Palandri and Kharaka, 2002, 2003a, 2003b; Palandri and Kharaka, in press). However, there is uncertainty in the relative and absolute rates of iron carbonate, iron sulfide and native sulfur precipitation, which are of particular importance. It is necessary for the rate of carbonate precipitation to be fast relative to the precipitation of solid iron sulfide and native sulfur. If iron sulfide initially precipitates, the rate of its conversion to iron carbonate is likely to be slow, and if native sulfur precipitates early the rate of sulfur dissolution and oxidation accompanied by iron reduction is also likely to be slow. Further, the absolute rate of iron carbonate formation should be sufficiently fast, to fix CO<sub>2</sub> in minerals and prevent the return of CO<sub>2</sub> to the Earth's surface. Below, we compare the results from an equilibrium simulation to results from an experiment with identical temperature, pressure and composition, to investigate possible departure from equilibrium arising from kinetic control of the chemical reaction rates.

## 2. METHODS

We constructed an equilibrium geochemical simulation and an experiment using identical initial parameters except for the quantity of SO<sub>2</sub>. The simulation provides a measure of the degree to which the experiment approaches equilibrium. Conditions were 150°C and 300 bar. The initial aqueous phase was 150 ml of 1.0m NaCl, 0.5m NaOH brine; NaOH was used to increase pH and thus the initial degree of siderite supersaturation and its precipitation rate. The solid phase was 10g of hematite. The amount of anhydrous CO<sub>2</sub> was 16g, a quantity sufficient to ensure the existence of a supercritical gas phase over the course of the reaction. The experiment used a fixed 2.5 g amount of SO<sub>2</sub>, and the simulation was constructed using incrementally increasing amounts of SO<sub>2</sub> from 0.0 to 50g.

### 2.1 Modeling

The equilibrium simulation was computed using CHILLER (Reed, 1998), which calculates the distribution of chemical components among minerals, gases and species in the aqueous phase. CHILLER computes aqueous activity coefficients using the extended Debye-Hückel equation of Helgeson, et al. (1981), as modified by Tanger and Helgeson (1988). CHILLER uses a virial equation (Spycher and Reed, 1988) to compute the fugacity coefficients for H<sub>2</sub>O, CO<sub>2</sub>, CH<sub>4</sub>, and mixtures thereof, and for H<sub>2</sub> alone; data are not available to compute the fugacity coefficients for SO<sub>2</sub> or H<sub>2</sub>S and ideality is assumed. However, because SO<sub>2</sub> and H<sub>2</sub>S are very soluble in aqueous fluids, the amount of these components in the gas phase is negligible. A further limitation is that the calculation of equilibrium constants is limited to conditions along the H<sub>2</sub>O liquid-vapor saturation curve. However variations in the equilibrium constants due to pressure change are quite small compared to those due to temperature change. In the CHILLER thermodynamic database, mineral data are derived from the data of Holland and Powell (1998), and aqueous species data are derived from the SUPCRT92 database of Johnson et al. (1992).

The brine was first equilibrated with hematite at the stated conditions, yielding small quantities of dissolved ferric iron and a computed pH of 10.9. The system was then equilibrated with excess (supercritical) CO<sub>2</sub>, yielding a pH of 5.9. The simulation was then completed by adding SO<sub>2</sub> incrementally to obtain the results discussed below.

## 2.2 Experimental

### 2.2.1 Experimental Apparatus and Set-Up

The experiment was carried out in a flexible gold reaction cell with ~200cc total volume, that allows sampling of the fluid while maintaining experimental temperature and pressure conditions. The cell was contained within an autoclave which in turn was contained in a cyclic rotating (180°) furnace. The brine (150ml @ 25°C, sparged with N<sub>2</sub>) and hematite (75-125 μm size fraction; from Minas Gerais, Brazil, obtained from Ward's Natural Science Establishment) were sealed inside the cell/autoclave/furnace assembly, and pressurized to 100 bar. The pressure is controlled by adding or removing water from an annulus that surrounds the gold cell inside the autoclave. The CO<sub>2</sub> was injected with a syringe pump, and the assemblage was heated to 150°C, and the pressure was adjusted to 300 bar. The SO<sub>2</sub> was then added with the syringe pump. Because of the high compressibility of SO<sub>2</sub> and the small volume used, there is a high degree of uncertainty in the amount added.

### 2.2.2 Analytical

Aqueous samples were withdrawn periodically from the experiment for chemical analysis. Fluid pH was determined immediately; reported pH values are maxima because the fluid samples degas CO<sub>2</sub> and the pH increases upon sampling. Dissolved sulfate and thiosulfate concentrations were determined by ion chromatography. Total and ferrous iron concentrations were determined by the ferrozine colorimetric method (Stookey, 1970), and ferric iron was calculated from the difference. Solids were analyzed by X-ray diffraction and scanning electron microscope with energy dispersive spectroscopy (SEM/EDS) to obtain backscatter images and semi-quantitative mineral chemical compositions.

## 3. RESULTS

### 3.1 Modeling

Siderite is stable over a wide range of total added SO<sub>2</sub> gas (Fig. 1A), from -6.3 to 1.2 log grams (1 μg to 16 g). Pyrite replaces siderite, but only after hematite has dissolved completely. Sulfur eventually replaces pyrite between 25 and 35g of added SO<sub>2</sub> gas (Fig. 1A, off-scale right.)

Note that selected minerals may be suppressed where less stable phases are expected to precipitate because of their relative precipitation kinetics. Examples include suppression of quartz where amorphous silica is expected, or of pyrite and pyrrhotite where amorphous FeS is expected. Pyrite is not suppressed to show that the most stable of the iron sulfides (pyrite) is a less stable repository for iron than siderite. If pyrite and pyrrhotite are suppressed (not shown), then sulfur precipitates directly after siderite dissolution, and amorphous iron sulfide does not precipitate.

The pH is nearly constant at ~5.9 (Fig. 1B) until hematite begins to dissolve out because of pH buffering by carbonate/bicarbonate, and because hematite dissolution consumes copious H<sup>+</sup>. A significant finding is that the total dissolved sulfide concentration, dominated by H<sub>2</sub>S, remains less than 10 ppb until siderite dissolves completely, then increases to ~30-300 ppm where pyrite is stable, and ~600 ppm where native sulfur is stable. The dissolved iron concentration, predominantly as the ferrous iron-bearing species Fe<sup>2+</sup>, FeCl<sup>+</sup> and FeSO<sub>4</sub>, also remains low, at ~1.0 ppm until hematite begins to decrease, then increases sharply to ~31000 ppm as siderite dissolves, then to 34000 ppm as pyrite dissolves.

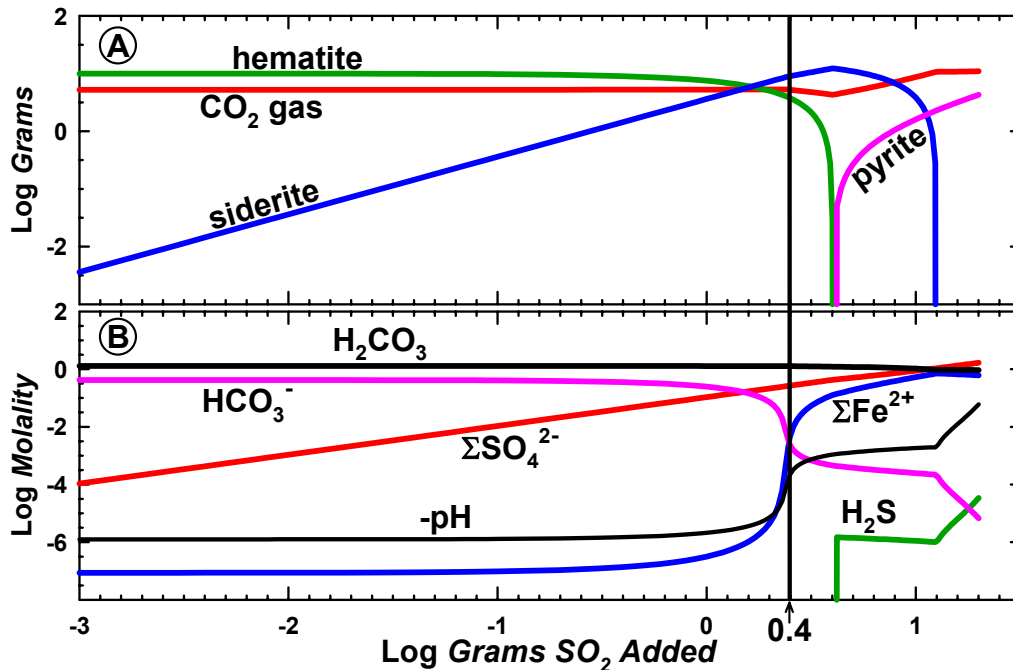


Figure 1: Summary of the results from the simulation of the CO<sub>2</sub>-SO<sub>2</sub> reaction with hematite in brine; vertical line at 0.4 log grams (2.5 g) represents the quantity of SO<sub>2</sub> used in the experiment. A) Mineral/gas phase assemblage. B) Fluid composition.

The vertical line at 0.4 log grams (2.5g) added SO<sub>2</sub> denotes the system composition and distribution of species used in the experiment. Therefore, if the experiment reaches equilibrium, then the mineral assemblage should contain only hematite and siderite. Further, for any amount of SO<sub>2</sub> gas added, the existence of hematite or of iron sulfide are mutually exclusive.

A significant limitation in using ferric iron to trap CO<sub>2</sub> is that the desired molar ratio for CO<sub>2</sub> to SO<sub>2</sub> indicated by equation (4) is 2:1. However, the ratio in the simulation where all of the hematite has been consumed is near 3:1 (excluding the gas phase) because a large amount of CO<sub>2</sub> is dissolved in solution. In either case, flue gas derived from the combustion of fossil fuel, even coal with high sulfur content, typically contains less than 1.0 wt% SO<sub>2</sub>, and would not contain enough SO<sub>2</sub> to reduce iron in quantity sufficient to trap all of the CO<sub>2</sub> in siderite. Therefore targeted sediments should contain other divalent metals capable of precipitating carbonate minerals, e.g. Ca or Mg. Alternatively, sulfur-bearing waste gas derived from other industrial processes, e.g. H<sub>2</sub>S from sour natural gas production, could be added to the waste gas stream.

### 3.2 Experimental

The fluid composition over the course of the experiment is summarized in Figure 2. Iron concentrations (Fig. 2A) are initially quite high because we neglected to wash the hematite sample to remove the small particles after grinding. The total iron concentration after 17 hours is 315 ppm, which decreases rapidly to 12 ppm after 38 hours. Total iron then increases to 447 ppm at 611 hours, then decreases to 190 ppm, and remains approximately constant for the remainder of the experiment. Total dissolved iron is dominated by ferrous iron rather than ferric iron over the course of the experiment. In the two instances where iron begins to decrease at 17 and 611 hours, it is apparent that dissolved iron has increased to a point where nucleation of an iron-bearing mineral has occurred and growth is proceeding. Given that nucleation and growth of amorphous iron is fast (Palandri, 2000) and siderite is relatively slow

(Greenberg and Tomson, 1992), it is likely that initiation of precipitation of iron sulfide has occurred near 17 hours, and of siderite near 611 hours.

Concentrations of dissolved sulfur species are shown in Figure 2B. Disproportionation leads to large concentrations of sulfate and thiosulfate after 17 hours. Sulfite was also detected but was not quantified because the eluent for the ion chromatograph was in equilibrium with atmospheric O<sub>2</sub> leading to oxidation of sulfite. The odor of sulfide was not detected in any of the fluid samples over the course of the experiment. Sulfur not represented in Figure 2B is likely contained in dissolved sulfite, dissolved SO<sub>2</sub>, or solid native sulfur.

The fluid pH was measured as quickly as possible after fluid sampling. The pH values shown in Figure 2C are maxima because the fluid degasses CO<sub>2</sub> upon sampling, leading to increased pH. However, decreased pH values centered around 4.3 at 323 hours appears to be a real effect resulting from the SO<sub>2</sub> reaction with water to produce sulfuric acid, with (H<sub>2</sub>) or without disproportionation (SO<sub>3</sub><sup>-</sup>, SO<sub>4</sub><sup>2-</sup>, HS<sup>-</sup>). The pH then recovers to its original values apparently due to hematite dissolution which consumes copious H<sup>+</sup>.

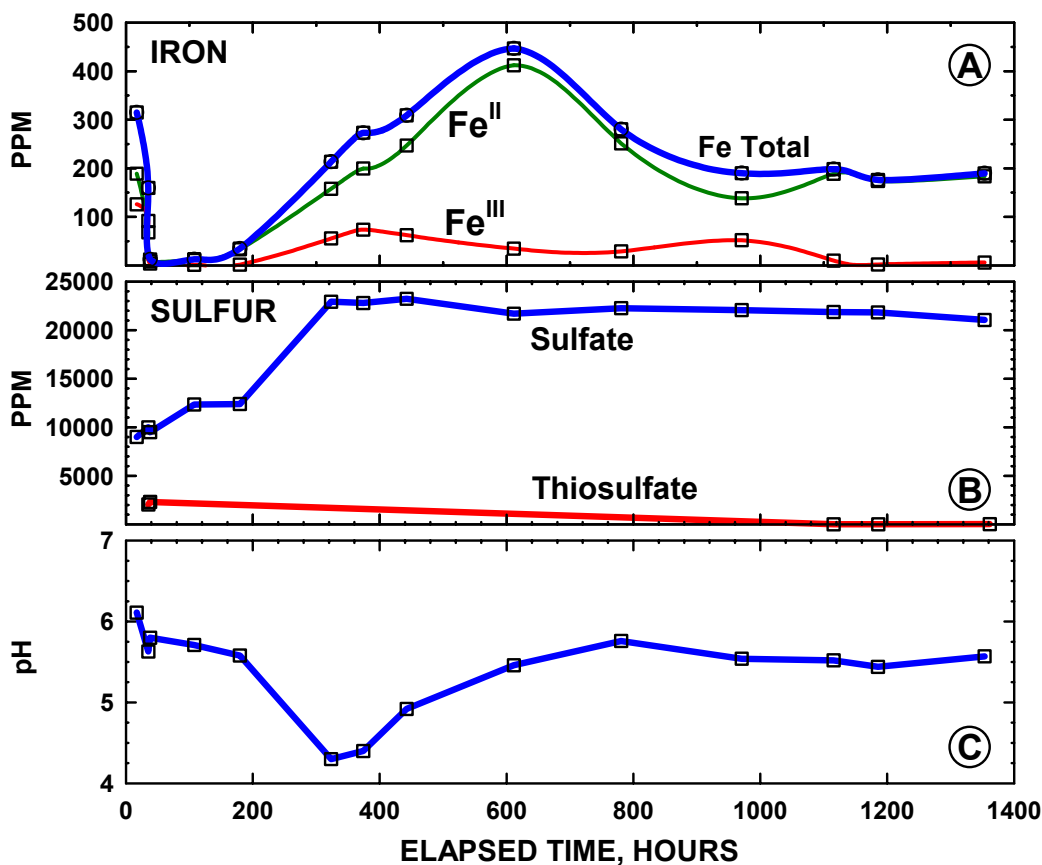


Figure 2: Experimental reaction of CO<sub>2</sub>-SO<sub>2</sub> with hematite in brine, fluid composition. A) Dissolved iron: total iron, ferrous iron, ferric iron. B) Dissolved sulfur: sulfate, thiosulfate. C) Fluid pH, maximum values due to CO<sub>2</sub> degassing upon sampling.

Analyses of the solids from the experiment show that mixtures of CO<sub>2</sub> and SO<sub>2</sub> can be used to reduce ferric iron to ferrous iron, and precipitate the ferrous iron in siderite. Alteration minerals include siderite, solid iron sulfide, dawsonite, and native sulfur. X-ray diffraction spectra verify the presence of hematite and pyrite only, and SEM/EDS verifies the presence of the other reaction products (Figs. 3-7.) In

comparison of the simulated and experimental alteration assemblages, coexistence of solid iron sulfide and sulfur with siderite clearly indicates that experiment is far from equilibrium after almost two months.

All of the hematite grains show some evidence of etching, but most do not show the presence of the alteration minerals on their surface. Other hematite grain surfaces show the presence of siderite, dawsonite and iron sulfide (Figs. 3 and 4.) Further, we observed discrete hematite-free clumps composed of siderite and native sulfur (Figs. 5 and 6). Siderite partially enclosed by sulfur suggests that the sulfur continued to grow after nucleation and growth of siderite. Other siderite crystals appear to be growing on the surface of the sulfur; these siderite crystals may have precipitated from: 1) ferrous iron already in solution, 2) ferrous iron derived from ongoing iron reduction by already-dissolved reduced sulfur (as thiosulfate or sulfite), or 3) from ferrous iron derived from ongoing iron reduction by dissolved sulfur derived from back-reaction and dissolution of the native sulfur or solid iron sulfide.

The solids contain extremely fine-grained native sulfur and solid iron sulfide (Fig. 7). This conclusion is reached based on EDS analysis showing the presence of both iron and sulfur, and optical microscopy showing mostly gray-black mineral grains, and a small number of yellow S grains in the mixture.

The computer simulation discussed above indicates that siderite and iron sulfide or sulfur cannot coexist at equilibrium. Their coexistence in the experiment indicates metastability but not equilibrium. This can be attributed to the slow dissolution rate of hematite. It is likely that with time the metastable native sulfur would dissolve, and possibly metastable iron sulfide as well, leading to further reduction of ferric iron in hematite and further precipitation of siderite.

A small amount of dawsonite was detected as shown Figures 3 and 4. Results from X-ray diffraction spectroscopy show only the presence of hematite in the initial material. However, hematite can take up significant amounts of  $\text{Al}_2\text{O}_3$  in solid solution, e.g. 10 wt% at  $1000^\circ\text{C}$  (Deer et al., 1992). Alternatively, aluminum is contained in other phase(s) present in quantities insufficient to be detected by X-ray diffraction.



**Figure 3: SEM backscatter image (x2000 magnification) of solids from the experiment. Sid, siderite; D, dawsonite; FeS, iron sulfide (pyrite or amorphous FeS); H, hematite.**

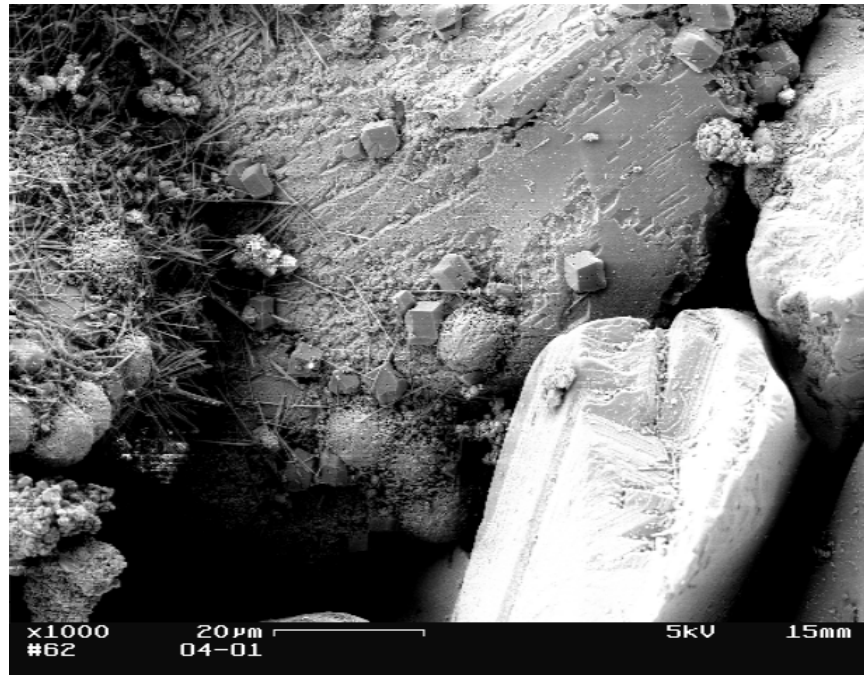


Figure 4: SEM backscatter image of solids from the experiment. As in Figure 3, at lower magnification, x1000.

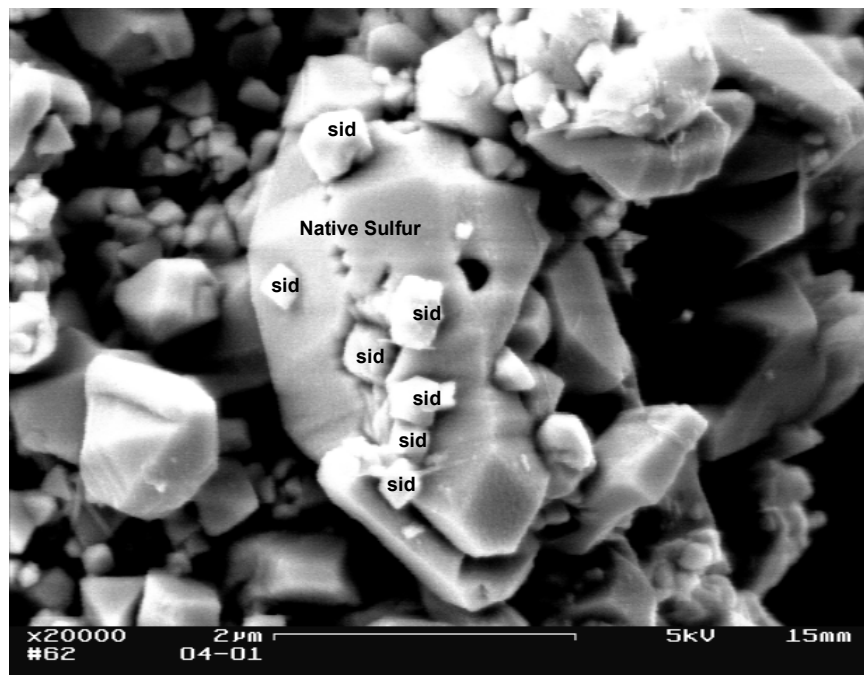


Figure 5: SEM backscatter image (x20000 magnification) of solids from the experiment. Siderite (sid) crystals growing on native sulfur. Siderite has apparently nucleated after nucleation and growth of native sulfur.

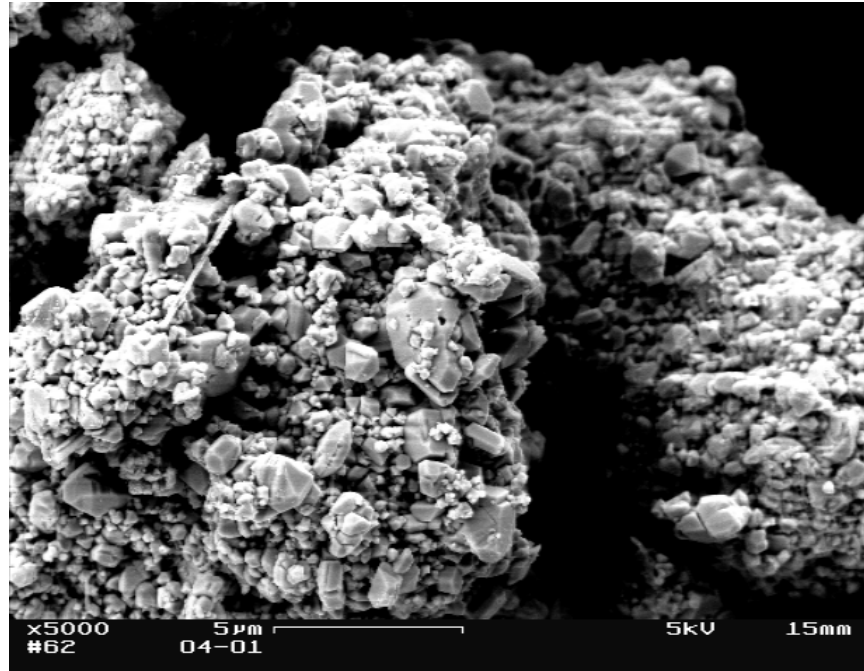


Figure 6: SEM backscatter image of solids from the experiment. As in Figure 5, at lower magnification, x5000.

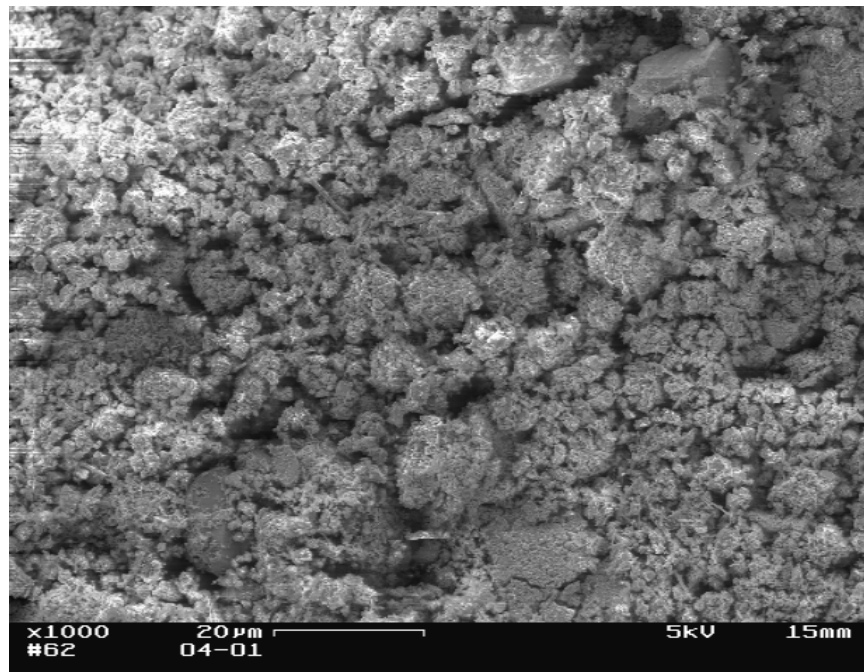


Figure 7: SEM backscatter image of solids from the experiment. EDS indicates the presence of iron and sulfur. Optical microscopy indicates two extremely fine-grained minerals, most gray-black and some yellow in color, apparently a mixture of mostly iron sulfide and a small amount of native sulfur.

#### 4. CONCLUSIONS

The results predicted by the computer simulation are confirmed by the experiment. Mixtures of CO<sub>2</sub> and SO<sub>2</sub> gas will react with ferric iron in hematite, in aqueous phase reactions, to produce the ferrous iron carbonate mineral siderite. However, the experiment did not reach equilibrium after two months, as indicated by the presence of two metastable phases, solid iron sulfide and native sulfur. In the experimental fluid, metastable thiosulfate and metastable sulfite were also detected, which decreased with time. Experimental results are consistent with nucleation of solid iron sulfide at 38 hours, nucleation of native sulfur before 611 hours, and nucleation of siderite at 611 hours.

Further experimental investigation of the reaction is warranted. Suggestions to improve further work include: 1) use of a smaller size fraction of hematite (38-75µm or smaller) and possibly higher temperatures to increase the reaction rates; 2) allowing experiments to run for much longer periods of time; 3) addition of SO<sub>2</sub> in increments over the course of the experiment rather than adding all SO<sub>2</sub> initially, to limit native sulfur precipitation; 4) parallel experiments with and without NaOH to simulate presence and absence of natural rock components that may buffer pH; 5) parallel experiments with and without use of Ca- and Mg-bearing natural rock pH buffers; 6) additional analyses of the fluid for thiosulfate, sulfite, and sulfide; 7) preservation of fluid samples with an anti-oxidant buffer to prevent oxidation of reduced sulfur-bearing species in the fluid such as thiosulfate, sulfite, and sulfide; 8) for the same reason, use of ion chromatograph eluent with an anti-oxidant buffer; and 9) use of an in situ pH electrode to obtain pH measurements at the experimental conditions.

**Acknowledgements**—We thank Gil Ambats, Monami Datta, Mark Huebner, Evangelos Kakouros, and Andy Ouimette for their assistance in preparation of the initial experimental solids and in sampling and analysis of the experimental fluids. We also thank Robert Oscarson for his assistance with the SEM/EDS in analysis of the experimental solids.

#### REFERENCES CITED

- Deer W. A., Howie R. A., and Zussman J. (1992) *An Introduction to the Rock-Forming Minerals*. Longman, Essex.
- Getahun A., Reed M. H., and Symonds R. (1996) Mount St. Augustine Volcano fumarole wall rock alteration: mineralogy, zoning, composition and numerical models of its formation process. *Journal of Volcanology and Geothermal Research* **71**, 73-107.
- Greenberg J. and Tomson M. (1992) Precipitation and dissolution kinetics and equilibria of aqueous ferrous carbonate vs temperature. *Appl. Geochem.* **7**, 185-190.
- Gunter W. D., Perkins E. H., and Hutcheon I. (2000) Aquifer disposal of acid gases: modelling of water-rock reactions for trapping of acid wastes. *Appl. Geochem.* **15**, 1085-1095.
- Gunter W. D., Wiwchar B., and Perkins E. H. (1997) Aquifer disposal of CO<sub>2</sub>-rich greenhouse gases: Extension of the time scale of experiment for CO<sub>2</sub>-sequestering reactions by geochemical modeling. *Mineralogy and Petrology* **59**, 121-140.
- Helgeson H. C., Kirkham D. H., and Flowers G. C. (1981) Theoretical prediction of the thermodynamic behavior of aqueous electrolytes at high pressures and temperatures: IV. Calculation of activity coefficients, osmotic coefficients, and apparent molal and standard and relative partial molal properties to 600°C and 5kb. *Am. J. Sci.* **281**, 1249-1516.
- Holland T. J. B. and Powell R. (1998) An internally consistent thermodynamic data set for phases of petrological interest. *J. Metamorph. Geol.* **16**, 309-343.

- Johnson J. W., Nitao J. J., Steefel C. I., and Knauss K. G. (2001) Reactive transport modeling of geologic CO<sub>2</sub> sequestration in saline aquifers: the influence of intra-aquifer shales and the relative effectiveness of structural, solubility, and mineral trapping during prograde and retrograde sequestration. *First National Conference on Carbon Sequestration*. May 14-17, 2001, Washington, D.C. 60 pp.
- Johnson J. W., Oelkers E. H., and Helgeson H. C. (1992) SUPCTR92: A software package for calculating the standard molal thermodynamic properties of minerals, gases, aqueous species, and reactions from 1 to 5000 bar and 0 to 1000°C. *Computers & Geosciences* **7**, 899-947.
- Palandri J. L. (2000) Applications of computed chemical equilibria: I. Reconstruction of in situ composition of sedimentary formation waters; II. Disposal of H<sub>2</sub>S from natural gas; III. Serpentinization, related rodingitization, and silica-carbonate alteration of ultramafic rock. Ph.D. Thesis, University of Oregon. 384 pp.
- Palandri J. L. and Kharaka Y. K. (2002) Ferric iron-bearing sediments as a mineral trap for geologic CO<sub>2</sub> sequestration: Iron reduction using SO<sub>2</sub> or H<sub>2</sub>S waste gas. *EOS, Trans. AGU*, **83(47)**, Fall Meet. *Suppl., Abstract U21A-05*.
- Palandri J. L. and Kharaka Y. K. (2003a) Ferric iron minerals as geologic traps for CO<sub>2</sub> sequestration: Iron reduction using sulfur-bearing waste gas. *National Energy Technology Laboratory Second Annual Conference on Carbon Sequestration*. May 5-8, 2003, Alexandria, VA.
- Palandri J. L. and Kharaka Y. K. (2003b) Ferric iron-bearing minerals as geologic traps for CO<sub>2</sub> sequestration: iron reduction using SO<sub>2</sub> or H<sub>2</sub>S waste gas. *Abstracts with Programs - American Association of Petroleum Geologists* **12**, A131.
- Palandri J. L. and Kharaka Y. K. (In Press) Sequestration of CO<sub>2</sub> in Redbeds: Siderite Precipitation from CO<sub>2</sub> and SO<sub>2</sub> Waste Gas. In *Proceedings of the 7th international symposium on water-rock interaction*.
- Pruess K., Xu T., Apps J., and Garcia J. (2001) Numerical Modeling of Aquifer Disposal of CO<sub>2</sub>. *SPE/EPS/DOE Exploration and Environmental Conference* San Antonio, Texas. pp. 1-14.
- Reed M. H. (1998) Calculation of simultaneous chemical equilibria in aqueous-mineral-gas systems and its application to modeling hydrothermal processes. In *Techniques in Hydrothermal Ore Deposits Geology* (eds. J. Richards and P. Larson). Economic Geology, Socorro, NM. pp. 109-124.
- Spycher N. F. and Reed M. H. (1988) Fugacity coefficients of H<sub>2</sub>, CO<sub>2</sub>, CH<sub>4</sub>, H<sub>2</sub>O and of H<sub>2</sub>O-CO<sub>2</sub>-CH<sub>4</sub> mixtures: A virial equation treatment for moderate pressures and temperatures applicable to calculations of hydrothermal boiling. *Geochim. Cosmochim. Acta* **52**, 739-749.
- Stokey L. L. (1970) Ferrozine-A New Spectrophotometric Reagent for Iron. *Anal. Chem.* **42**, 779-782.
- Symonds R., Gerlach T., and Reed M. (2001) Magmatic gas scrubbing: Implications for volcano monitoring. *Journal of Volcanology and Geothermal Research* **108**, 303-341.
- Tanger J. C., IV and Helgeson H. C. (1988) Calculation of the thermodynamic and transport properties of aqueous species at high temperatures and pressures: Revised equations of state for the standard and partial molal quantities of ions and electrolytes. *Am. J. Sci.* **288**, 19-98.